Multiple scattering of MeV light ions through thin amorphous anodic SiO_2 layers formed on silicon single crystals

D. Schmaus, F. Abel, M. Bruneaux, C. Cohen, and A. L'Hoir
Groupe de Physique des Solides de l'Ecole Normale Supérieure, Université Paris VII, Tour 23, 2 place Jussieu, 75221 Paris Cedex 05, France

G. Della Mea, A. V. Drigo, S. Lo Russo
Istituto di Fisica dell'Università, Unità del Gruppo Nazionale di Struttura della Materia, Padova, Italy

G. G. Bentini
Laboratorio per la Chimica e Tecnologia dei Materiali e Componenti per l'Elettronica, Consiglio Nazionale delle Ricerche, Bologna, Italy

(Received 5 June 1978)

The multiple-scattering angular distributions of protons, helium, and nitrogen ions between 500 keV and 2 MeV which have passed through anodic SiO_2 films (in the 100–1500-Å thickness range) formed on the top of [110] Si single crystals have been determined. They were obtained by comparing, at different penetration depths, the backscattering yields in Si crystals covered by SiO_2 layers to the azimuthally averaged yields in a bare crystal at various angles of incidence with respect to the [110] axis. The precision and limits of the method used are discussed. The detailed and precise experimental data on channeling in silicon which are required are reported. The experimental distributions are compared to the theoretical predictions obtained by extension of the Bothe's formula to diatomic targets and using a scattering cross section corresponding to the Thomas-Fermi potential. In the particular case of SiO_2, the theoretical distributions are shown to be nearly identical to the distributions calculated for a monoatomic target of atomic number $Z = 10$. Very good agreement is observed, for protons and helium, between the experimental and the theoretical distributions when the Thomas-Fermi screening radius of the target atoms is used. This screening radius is well adapted to our experimental cases since, in our energy domain, protons and helium have a very high probability to be completely stripped in matter.

I. INTRODUCTION

The growing interest in techniques involving ion beams has developed a demand for detailed information on particle-matter interaction. Since the major contribution of Bohr,[1] who has given a large survey of the whole subject, detailed theoretical and experimental studies have been undertaken on various aspects of the problem. One of the points of interest is the angular distribution of a beam of particles which has passed through a given thickness of matter. This distribution is governed by multiple-scattering events with the target atoms. In particular, multiple scattering is of fundamental importance in determining the trajectory of implanted ions; it intervenes as a limiting factor in the depth resolution of backscattering or nuclear-microanalysis experiments when grazing incidence or emergence geometry are used in order to investigate the very near surface region of a solid; it has to be taken into account in the interpretation of most channeling data since, generally, the particles have to go through an amorphous surface layer before entering the crystal.

The precise knowledge of multiple-scattering distributions is also needed for the data reduction of experiments in beam-foil or beam-gas spectroscopy. The angular spread of the stripped beams passed through thin foils in tandem accelerators is also a typical technical problem which requires information on multiple scattering.

The theoretical treatment of multiple scattering requires the knowledge of the individual-scattering cross sections, i.e., of the interatomic potential. A statistical treatment based on the assumption of a random homogeneous distribution of the scattering centers and of independent binary collisions is then usually introduced. These assumptions are well verified for a dilute gas whereas they should be carefully discussed for a solid. In the experiments performed in the latter case (see, for instance, Refs. 2 and 3), some discrepancies were found with respect to the theoretical predictions. However, it must be pointed out that these discrepancies appear for polycrystalline samples; moreover, thickness-

homogeneity problems may arise for the very thin self-supporting targets which were used in the transmission-type experiments reported. Hence the disagreement between these experiments and theory cannot be systematically attributed to the interatomic potential used or the statistical treatment introduced in the theory.

We report here experiments performed in order to measure the multiple-scattering distribution of MeV light particles passed through thin uniform amorphous films. These films were not self-supporting, but formed on the top of thick single crystals. The method used to determine the angular distributions of the particles passed through the films was first proposed by Rimini *et al.*[4] It consists in comparing the "aligned" backscattering yield of the particles in the crystals covered by the films to the backscattering yields measured at various incident angles with respect to a major crystallographic axis on a bare crystal. The amorphous films used in our experiments were SiO_2 layers formed by anodic oxidation of silicon crystals. These layers were shown to be amorphous and of high thickness uniformity[5–7]; moreover, this thickness can be determined within a ±3% absolute precision using oxygen nuclear microanalysis.[8] The study of multiple scattering through diatomic films was of particular interest since very few experiments on the subject have been performed (some results were reported on Ta_2O_5 in Ref. 2) and no calculated angular distributions are available in this case.

The backscattering yields as a function of angle of incidence on bare silicon crystals had to be measured with great precision in order to extract information on multiple scattering; they are reported in Sec. V. Detailed information was obtained on the channeling of H, ^{4}He, ^{14}N ions in silicon; various beam energies between 500 keV and 2 MeV were used. The results on critical angles, minimum yield, and dechanneling phenomena were expressed in reduced coordinates in order to evidence universal laws; we also report a comparison with the measurements and calculations of other authors.

The theoretical multiple-scattering distributions for SiO_2 targets are calculated in Sec. III, and compared in Sec. VII to the angular distribution extracted from our experimental results. The limits and precision of the method are discussed in Sec. VI.

The results and analysis of the present paper were already developed in the thesis of Schmaus.[9]

II. PRINCIPLES

Passing through an amorphous layer deposited or formed on the top of a single crystal, particles are scattered at various angles. If a major axis of the single crystal is aligned with the incident beam, the proportion of channeled particles is a decreasing function of the thickness of the amorphous layer. The backscattering minimum yield χ^{ox} for a crystal covered with an amorphous layer is related to the angular distribution $2\pi\phi F(\phi)$ of particles having passed through this layer by

$$\chi^{ox} = \int_0^{2\pi} \frac{d\omega}{2\pi} \int_0^{\infty} 2\pi\phi F(\phi)\chi_\omega^b(\phi)\,d\phi = \int_0^{\infty} 2\pi\phi F(\phi)\chi^b(\phi)\,d\phi \quad . \tag{1}$$

In this relation $\chi_\omega^b(\phi)$ is the yield measured on a bare crystal for a beam impinging at an angle ϕ with respect to the crystallographic axis, the crystal being in an azimuthal position defined by ω.

$\chi^b(\phi)$ is then the aximuthally averaged yield for the incident angle ϕ. The yields $\chi_\omega^b(\phi)$ depend strongly on the azimuthal position ω, since planar channeling effects arise; as on the other hand, the angular distribution of the particles passed through the amorphous layer has circular symmetry with respect to the incident direction, the averaging over all the azimuthal position of $\chi_\omega^b(\phi)$ must be undertaken. The way the azimuthally averaged yields $\chi^b(\phi)$ were experimentally obtained is described in Sec. IV.

The basic assumption leading to Eq. (1) is the equality of the backscattering yields at the same angle of incidence on the bare crystal and on the crystal covered with the amorphous layer. Therefore the crystalline quality of the two crystals is assumed to be identical. In our experiments all the silicon single crystals used were cut in the same wafer. The amorphous layer was silicon oxide formed by anodic oxidation; it seems reasonable to assume that this process does not affect appreciably the crystal quality behind the oxide.

Lugujjo and Mayer[10] have used Eq. (1) to check the validity of the angular distributions tabulated by Meyer.[11] In their experiments, silicon crystals were covered by gold films formed by evaporation. They verified that for the backscattering yields at the crystal surface χ^{ox} and $\chi^b(\phi)$, Eq. (1) was well verified by the tabulated distributions. This result is in contradiction with the experiments reported in Ref. 2 where the measured angular distributions were found in some cases systematically narrower than the calculated ones, this fact being attributed to the polycrystallinity of the layers studied. Moreover the agreement obtained in Ref. 10 was also found to hold when the yields $\chi^b(\phi)$ used in Eq. (1) are approximated by a step function. In this approximation $\chi^b(\phi)=0$ for $\phi < \psi_{1/2}$ and $\chi^b(\phi)=1$ for $\phi > \psi_{1/2}$, where $\psi_{1/2}$ is the halfwidth at half maximum (HWHM) of the azimuthally averaged angular scan at the crystal surface. With this approximation Eq. (1) becomes

$$\chi^{ox} = \int_{\psi_{1/2}}^{\infty} 2\pi\phi F(\phi)\, d\phi \quad . \tag{2}$$

Hence, in the treatment of Ref. 10 any distribution $F(\phi)$ having a correct weight in the $[0, \psi_{1/2}]$ angular domain is satisfactory. Consequently this treatment does not give detailed information on the shape of the angular distributions.

A more precise study of the function $F(\phi)$ is possible if one takes into account the fact that Eq. (1) must be valid at any depth x in the crystal. The angular distribution must hence obey, for all x, Eq. (3):

$$\chi^{ox}(x) = \int_{0}^{\infty} 2\pi\phi F(\phi)\chi^{b}(\phi,x)\, d\phi \quad . \tag{3}$$

Rimini *et al.*[12] have checked the distributions tabulated by Meyer[11] by comparing the values $\chi^{ox}(x)$, obtained when these distributions were fed into Eq. (3), to experimental yields (^{4}He ions through Al and Au layers deposited on Si single crystals). The values $\chi^{b}(\phi,x)$ used in Ref. 12 were not azimuthally averaged but simply obtained from standard channeling experiments, i.e., values $\chi^{b}_{\omega}(\phi,x)$ for a fixed ω value were inserted in Eq. (3). The authors find a good agreement between their calculated and measured $\chi^{ox}(x)$ in the case of aluminum layers. However, for gold layers, discrepancies are observed which could not be detected from the study of the surface yields alone. A calculation of $\chi^{ox}(x)$ without using measured values of $\chi^{b}(\phi,x)$ is also proposed in Ref. 12: a given entrance angular distribution being assumed, the yields $\chi^{ox}(x)$ are obtained from a simplified dechanneling model and can be again compared to the experimental values. This latter procedure is more a check of the validity of the dechanneling model adopted than a study of the function $F(\phi)$. Similar treatments and experiments are described by Campisano *et al.* in Ref. 13 (H^+ ions through Al and Au layers on Si crystals). Here a good agreement is found between experimental and calculated $\chi^{ox}(x)$ even in the case of gold layers. The contradictions observed between various experiments on gold layers may not be without relation with the crystallographic texture of the gold films which may vary from one experiment to another. An interesting property of Eq. (3) is underlined and used in Ref. 13: if a square-well approximation is introduced for the yields $\chi^{b}(\phi,x)$, an analytical calculation of the function $F(\phi)$ fitting the experimental values $\chi^{ox}(x)$ can be performed. This point will be developed and discussed in Sec. VI.

In the present paper we have searched for the functions $F(\phi)$ which, inserted in Eq. (3), lead to calculated values of $\chi^{ox}(x)$ in optimal agreement with our experimental results for all the ranges of penetration depths into the crystal for which a backscattering yield could be measured. The values $\chi^{b}(\phi,x)$ introduced in Eq. (3) were the azimuthally averaged yields obtained in our experiments. The physical meaning and justification of the fitting procedure which is presented is discussed in Secs. VI and VII. The limits and precision of the method are also analyzed in Sec. VI.

III. THEORETICAL ANGULAR DISTRIBUTIONS IN POLYATOMIC TARGETS: CASE OF SiO_2

Contrary to the case of monoatomic targets, no tabulated data are available for multiple scattering in polyatomic targets. Hence, in order to compare our experimental results to theoretical predictions we had to extend the calculations to the case of SiO_2. This extension is presented in this section.

A general formula for multiple-scattering distributions has been derived by Bothe.[14] The hypotheses involved in this calculation are worth outlining. First of all, the treatment is made classically in the small angle approximation; on the other hand the scattering cross section, for a given scattering angle, is supposed to be constant. This second point implies that the energy loss of the ions is neglected. These first two points are somewhat related: if the energy loss of the ions is neglected, the treatment is only valid for relatively small thicknesses of matter and in this case the small angle approximation holds. There is a third assumption in the treatment which is physically the most important: the calculations are based on a model of binary collisions, mutually independent, and the number of these collisions is assumed to follow the Poisson law. This hypothesis is fully valid in the case of dilute atomic gases. For molecular gases the collisions with atoms of the same molecule are not independent and the problem must be reexamined by considering, for instance, a molecule as a whole scattering center; this has been done by Sigmund.[15] The situation is more complex in the case of solid targets. Obviously the model of independent collisions does not hold for single crystals and even for polycrystals. In these cases correlated events are of prime importance. This is the major reason of the discrepancies observed between experimental results on polycrystalline films and theoretical predictions obtained from Bothe's treatment. In the case of amorphous solid targets a more detailed discussion is required and the validity of the dilute-gas model will be discussed in a forthcoming paper. However, Sigmund[16] has already estimated that for rather thick amorphous solid films (i.e., in the thickness range corresponding to the experiment presented here) Bothe's treatment holds. We will hence use an extension of this treatment to polyatomic targets.

A universal formulation of the Bothe formula for any couple particle–monoatomic-target and at any energy has been derived by Meyer[11] by introducing reduced coordinates classically used in this type of problem.[17] This derivation is only valid if the intera-

tomic potential is assumed to have the form

$$U(R) = (Z_1 Z_2 e^2/R)\, u(R/a) \quad , \tag{4}$$

where Z_1 and Z_2 are, respectively, the atomic number of the particle and the target atoms, and e the electron charge; $u(R/a)$ is a screening function of universal form (i.e., depending on Z_1 and Z_2 only by the value of the screening radius a).

The universal formula giving the angular distributions is then, using the notations of Refs. 11 and 18,

$$2\pi\phi F(x,\phi)\, d\phi = \tilde{\phi}\, d\tilde{\phi} \int_0^\infty z\, dz\, J_0(z\tilde{\phi})\, e^{-\tau\Delta(z)} = \tilde{\phi}\, d\tilde{\phi}\, f_1(\tau, \tilde{\phi}) \tag{5}$$

with

$$\Delta(z) = \int_0^\infty d\tilde{\phi} \frac{f(\tilde{\phi})}{\tilde{\phi}^2} [1 - J_0(z\tilde{\phi})] \quad . \tag{6}$$

Here J_0 is the zero-order Bessel function of the first kind. The quantity τ is a reduced thickness defined as

$$\tau = \pi a^2 N x \quad , \tag{7}$$

Nx being the number of target atoms per surface unit. Typically $\tau \simeq 1$ corresponds to about 100 Å of a solid target. $\tilde{\phi}$ is a reduced angle related to the angle ϕ in the laboratory system by

$$\tilde{\phi} = \mu\phi = (Ea/2Z_1 Z_2 e^2)\phi \quad , \tag{8}$$

where E is the particle energy. The function $f(\tilde{\phi})$ is related to the scattering cross section which can be expressed, in the case of interatomic potentials given by Eq. (4), by the universal expression

$$d\sigma = \pi a^2 [f(\tilde{\phi})/\tilde{\phi}^2]\, d\tilde{\phi} \quad . \tag{9}$$

The universal function $f_1(\tau, \tilde{\phi})$ has been tabulated by Meyer[11] and Sigmund and Winterbon,[18] and allows one to obtain directly the angular distribution for every coupled ion-scattering center. Sigmund and Winterbon[18] have tabulated the function $f_1(\tau, \tilde{\phi})$ for two different analytical forms of the scattering function $f(\tilde{\phi})$ corresponding respectively to the Thomas-Fermi and Lenz-Jensen screening function $u(R/a)$. In the case of polyatomic targets, the situation is less comfortable since no universal formulation can be proposed. However, some simplifications may be obtained by introducing the parameter μ defined in Eq (8). For a scattering center indexed by i, we have

$$\mu_i = Ea_i/2Z_1 Z_{2i} e^2 \quad . \tag{10}$$

The Bothe formula extended to polyatomic targets can then be written as follows:

$$2\pi\phi F(x,\phi)\, d\phi = \phi\, d\phi \int_0^\infty s J_0(s\phi) \exp\left[-\sum_i \tau_i \Delta\left(\frac{s}{\mu_i}\right)\right] \quad . \tag{11}$$

The function $\Delta(z)$ appearing in (11) is given by Eq. (6) and is of course universal. However, the integral (11) has to be recalculated for each couple ion-polyatomic target considered. This obligation falls in the case of the power potential $U(R) \sim R^{-1/m}$ for which the scattering function $f(\tilde{\phi})$ takes a particular form leading to great simplifications. In this case, the screening function is given by[17]

$$u(R/a) = m k_m (a/R)^{1/m-1} \tag{12}$$

and the scattering function becomes simply

$$f(\tilde{\phi}) = \lambda_m \tilde{\phi}^{1-2m} \quad . \tag{13}$$

Introducing this expression of $f(\tilde{\phi})$ in the integral giving $\Delta(z)$, one gets

$$\Delta(z) = c_m z^{2m} \tag{14}$$

With this particular form of $\Delta(z)$ all the distributions $f_1(\tau, \tilde{\phi})$ corresponding to a given monoatomic target-ion combination, have the same shape, the reduced thickness τ acting only as a scaling factor. Being given a particular distribution $f_1(\tau_1, \tilde{\phi})$ corresponding to a given reduced thickness τ_1, one gets the distribution corresponding to a reduced thickness τ_2 by the relationship

$$f_1(\tau_2, \tilde{\phi}') = f_1(\tau_1, \tilde{\phi})(\tau_2/\tau_1)^{-1/m}$$

with

$$\tilde{\phi}' = \tilde{\phi}\left(\frac{\tau_2}{\tau_1}\right)^{1/2m} \quad . \tag{15}$$

For a polyatomic target, Eq. (11) becomes

$$2\pi\phi F(x,\phi)\, d\phi = \phi\, d\phi \int_0^\infty s\, ds\, J_0(s\phi) \exp\left[-c_m s^{2m} \sum_i \tau_i \mu_i^{-2m}\right] \quad . \tag{16}$$

This means that a polyatomic target is equivalent to a "mean" monoatomic target defined by the relation

$$\bar{\tau}\bar{\mu}^{-2m} = \sum_i \tau_i \mu_i^{-2m} \quad . \tag{17}$$

Hence, whatever the target thickness and composition, and whatever the nature and energy of the incident ions, all the angular distributions corresponding to a given power potential are identical in shape.

The situation is far more complicated in the case of the Thomas-Fermi or Lenz-Jensen screened poten-

tial; hence it is interesting to discuss to what extent the power-potential approximation holds.

For very small thicknesses of matter ($\tau \lesssim 0.1$), the mean number of collisions corresponding to impact parameters smaller than $3a$, is smaller than 1. These collisions will then contribute to the angular distribution only in the tail corresponding to single-scattering events. The body of the distributions ($\tilde{\phi} < 2\tilde{\phi}_{1/2}$), characteristic of multiple scattering, will be due to collisions with impact parameters $p \geq 3a$. For these large impact parameters, the Thomas-Fermi or Lenz-Jensen potentials trend asymptotically towards power potentials ($m_{TF} = 0.311$, $m_{LJ} = 0.191$). Hence the body of the distributions will always keep the same shape and the depth scaling factor will be given by (15).

For very great thicknesses ($\tau \gtrsim 100$), and if we assume that the energy loss of the incident ions can still be neglected, the number of collisions corresponding to impact parameters smaller than $\frac{1}{3}a$ is great compared to unity. These collisions, corresponding to relatively large scattering angles, will be of prime importance in the overall angular distribution. Since they correspond to small impact parameters, the corresponding interaction potential is not far from a purely Coulomb potential ($m \simeq 1$) and here again, the shape of the body of the angular distribution is unique. It can be shown that the angular distribution $f_1(\tau, \tilde{\phi})$ tends in this case towards a Gaussian, at least as far as the body of the distribution is concerned. However, it can be shown from probability theory, that in this limit case ($m \to 1$), the scaling factor is no more given by Eq. (15); the body of the distribution broadens like $(\tau \log \tau)^{1/2}$ instead of $\tau^{1/2}$.

For the intermediate values of reduced thicknesses, one has to consider collisions corresponding to an impact-parameter domain in which the Thomas-Fermi or Lenz-Jensen potentials cannot be assimilated to a power potential. However, locally, i.e., in a narrow domain around a given value of R/a, the screening function $u(R/a)$ can always be adjusted by a power potential, matching $u(R/a)$ and its derivative $du(R/a)/d(R/a)$. This leads to values of m and k_m [see Eq. (12)] which depend on R/a. If, for a given thickness of matter, the body of the angular distribution is mainly due to collisions corresponding to a restricted domain of impact parameters, it is possible to define for this thickness a power potential, corresponding to the Thomas-Fermi or Lenz-Jensen potential, which accounts fairly well for the body of the angular distribution. The validity of this hypothesis will now be checked.

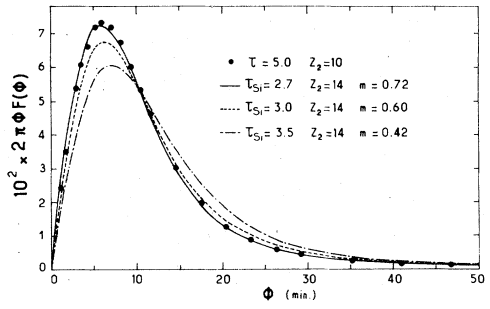

FIG. 1. Comparison, in the case of 1.8-MeV ^{4}He ions, of the angular distribution for a target characterized by $\tau = 5$ and $Z_2 = 10$ with the corresponding distributions obtained for various τ_{Si} calculated from Eq. (18), using different power potentials, in the case of a silicon target ($Z_2 = 14$).

If a power potential applies, the angular distribution corresponding to a reduced thickness τ_i of a monoatomic target indexed by i is equivalent to the angular distribution corresponding to a reduced thickness τ_j of a monoatomic target indexed by j, if the following relation is fullfilled [see Eq. (17)]:

$$\tau_i \left(\frac{Z_{2i}}{a_i}\right)^{2m} = \tau_j \left(\frac{Z_{2j}}{a_j}\right)^{2m} . \tag{18}$$

In Fig. 1 we compare, in the case of 1.8-MeV helium ions, the angular distribution obtained from the tables of Ref. 18 for a reduced thickness $\tau = 5$ of a specie of atomic number $Z_2 = 10$, to the angular distributions corresponding to various thicknesses of silicon ($Z_2 = 14$). For a given value of m, each reduced thickness of silicon τ_{Si} has been calculated from relationship (18). The distributions corresponding to the specie of $Z_2 = 10$ and to silicon are nearly identical when the value $m = 0.72$ is chosen. This value of m appears hence to be well adapted for reduced thickness around $\tau = 5$. Marwick and Sigmund[19] have derived a curve relating the reduced thickness τ and the appropriate power $-1/m$ by studying the variation with τ of the maximum value $f_1(\tau, 0)$ of the tabulated angular distributions. The value of m obtained in this way for $\tau \simeq 5$ is in good agreement with our result.

The agreement between the shape of angular distributions corresponding to $Z_2 = 10$ and to silicon is due to the fact that the atomic numbers of the two considered species are rather close. If Z_{2i} and Z_{2j} are very different, so will be τ_i and τ_j [see Eq. (18)]; the hypothesis of a constant value of m between τ_i and τ_j is hence no more valid and Eq. (18) cannot be used. This fact is illustrated in Fig. 2, which compares the angular distribution corresponding to $\tau = 2.7$ for $Z_2 = 14$, already represented in Fig. 1, to various distributions obtained for different thicknesses of different species, each thickness being determined by the Eq. (18), always using the value $m = 0.72$, which was shown to apply for $\tau \simeq 5$. The distributions corresponding to species of atomic number $Z_2 = 8$ (oxygen) and $Z_2 = 14$ (silicon) are

fairly close, the corresponding value of τ being of the same order of magnitude ($\tau_{Si}/\tau_{ox}=2.8$). However, for $Z_2=26$ and $Z_2=36$, the corresponding values of τ are one order of magnitude smaller than τ_{ox} and the corresponding angular distributions are markedly different.

Following Eq. (17), if a power potential can be used (i.e., if a unique value of m can be used), a diatomic compound, for instance SiO_2, can be replaced by a monoatomic material of atomic number $\bar{Z}_2$, equivalent from the point of view of multiple scattering. This can be done easily. One can for instance assume that $\langle Nx\rangle=(Nx)_{Si}+(Nx)_{ox}$ where $\langle Nx\rangle$ is the number of scattering centers of atomic number $\bar{Z}_2$ per unit area. With this assumption, $\bar{Z}_2$ is readily calculated from Eq. (17). The result is

$$[(Nx)_{Si}+(Nx)_{ox}]\bar{Z}_2^{2m}\bar{a}^{2-2m}=(Nx)_{Si}Z_{2Si}^{2m}a_{Si}^{2-2m}+(Nx)_{ox}Z_{2ox}^{2m}a_{ox}^{2-2m}\quad,\quad(19)$$

Where $\bar{a}$, corresponding to $\bar{Z}_2$, is calculated in the same way as a_{ox} or a_{Si}. When m varies from 1 to $\frac{1}{3}$, these values describing roughly a Thomas-Fermi potential, respectively, at very small and very large impact parameters $\bar{Z}_2$ calculated from Eq. (19), varies between 10.4 and 9.8. Hence a monoatomic target with $Z_2=10$ appears to be a very good approximation for SiO_2. This case is of course particularly favorable from this point of view. Considering the case of Ta_2O_5 gives rise to a much larger variation of $\bar{Z}_2$: to $m=1$ and $m=\frac{1}{3}$ corresponds, respectively, $\bar{Z}_2=40$ and $\bar{Z}_2=30$, this indicating that the description of Ta_2O_5 by a mean monoatomic target is not a good approximation. Hence, in the general case it is necessary for polyatomic targets to compute numerically the angular distributions from Eq. (11). This was done here although, as discussed above, the case of SiO_2 is particularly favorable, in order to check up to what extent the semiquantitative estimation of the equivalence between SiO_2 and a mean monoatomic target with $\bar{Z}_2=10$ holds.

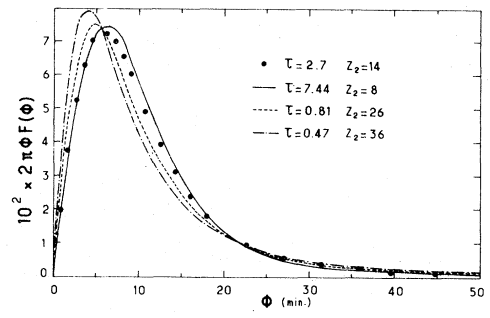

FIG. 2. Comparison, in the case of 1.8-MeV ^4He ions, of the angular distribution for $\tau=2.7$ and $Z_2=14$ with the angular distributions corresponding to various monoatomic targets. The reduced thickness τ of each target is calculated using Eq. (18) with a value of $m=0.72$.

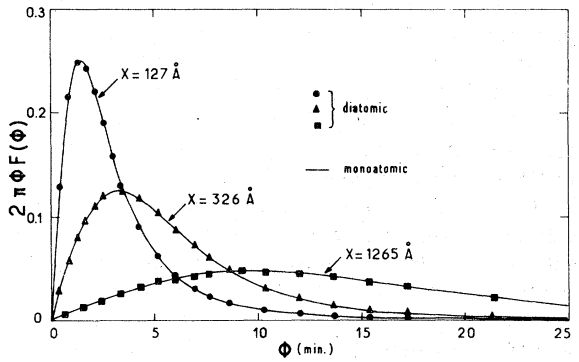

FIG. 3. Comparison of angular distributions for diatomic targets SiO_2 and monoatomic targets with $Z_2=10$. The distributions were computed for various target thicknesses in the case of 0.9-MeV protons.

For this purpose, a program was written. The aim was to obtain angular distributions for any polyatomic target with a good precision (better than 1%), in the reduced thickness domain $1\leq\tau\leq10$, up to angles 5 times the halfwidth at half maximum of the angular distributions. We had to compute the universal function $\Delta(z)$ for $10^{-3}<z<100$. The program was tested by comparing the results in the particular case $Z_{2i}=Z_{2j}$ to the tables of Ref. 18. The discrepancies are always small (less than 0.5%) for $\tau>1$, up to reduced angles $\tilde{\phi}$ about 4 times greater than the half width at half maximum of the angular distributions.

The comparison between the angular distribution computed by the program for SiO_2 and the angular distribution corresponding to a monoatomic target of $\bar{Z}_2=10$ containing the same number of scattering centers is illustrated in Fig. 3. In this figure, the comparison is done for various thicknesses of SiO_2 and in the case of 0.9-MeV protons. The agreement is very good, the discrepancies never exceeding 1% up to $\simeq3$ times the halfwidth at half maximum. This result confirms the semiquantitative discussion presented above. Hence it is possible to compare the angular distributions extracted from our experimental results to the tabulated distributions of Ref. 18.

IV. EXPERIMENTAL

A. Apparatus

The measurements were carried out with the 2-MeV Van de Graaff accelerator of the Groupe de Physique des Solides de l'Ecole Normale Supérieure. The beam handling system and electronic equipment are described in Ref. 20. In the experiments reported here, 900-keV H^+, 500- to 1800-keV $^4He^+$, and

1750-keV $^{14}N^+$ beams with currents of the order of some tens of nA were used. The energy resolution of the beam was about 300 eV. A series of diaphragms fixes the beam diameter at well-defined values in the range 0.5–2.0 mm while keeping the beam angular divergence [full width at half maximum (FWHM)] below 1 mrad.

The backscattered particles were detected by using a 25-mm^2 Ortec silicon surface-barrier detector. This detector was placed at an angle of 165°, with respect to the beam direction and at a distance of 7 cm from the sample. A 3-mm diam. diaphragm limited the solid angle to about 1.4 msr and the kinematic energy spread to less than 4 keV. The total energy resolution (FWHM) was found to 9 and 13 keV for protons and ^{4}He ions, respectively. The energy dependence of these energy resolutions is very weak in our energy range. On the contrary this dependence is marked for nitrogen ions. For the 1750-keV nitrogen beam used in this work we measured an energy resolution of 50 keV in good agreement with Ref. 21. The depth resolutions are around 300, 750, and 1100 Å for helium, nitrogen, and hydrogen ions, respectively.

The experiments were carried out on the goniometric chamber described in Ref. 22. The main advantage of this chamber for the present work is that a crystallographic axis of a sample can be aligned with the azimuthal rotation axis of a revolving stage with a $\pm 1'$ precision. The azimuthal rotation of the samples can be performed while keeping constant the angle between this crystallographic axis and the beam. As seen in Sec. II, this is of fundamental importance; the quantities of interest being the azimuthally averaged backscattering yields. Carbon buildup and radiation damage effects are strongly minimized if the beam impact point on the sample may be changed. For this purpose, the samples were mounted on an X-Y table; the translation keeps the misalignment below 1′.

The limit vacuum obtained in the chamber using a turbomolecular pump and a liquid-nitrogen trap is about 2×10^{-7} Torr.

The whole chamber is well insulated and can act as a Faraday cup. The total charge received by the sample can be measured by a low-impedance current integrator. In our experiments, however, the sample needs to be nearly continuously rotated and this could lead to integration of spurious currents due to the pulses sent to the goniometer stepping motors. The beam dose was hence measured using a beam chopper described in Ref. 23: this dose was obtained by integrating the spectra of particles backscattered by a gold layer deposited on sectors of the rotating wheel. About 25% of the incoming beam was intercepted. The azimuthally averaged spectra were obtained by addition of the spectra corresponding to various fixed azimuthal positions. The distance between two consecutive positions corresponded to 0.25′, i.e., one step of the motor. The rotation of the sample was monitored by a preset scaler, counting the pulses corresponding to the particles backscattered on the chopper; this ensured the constancy of the beam dose received by the sample for each azimuthal position.

B. Sample preparation and characterization

The samples were silicon wafers cut perpendicular to the [110] axis. The natural surface oxide and organic contamination on the "bare" crystals were minimized by successive dipping in H_2SO_4 and HF and rinsing in distilled water and acetone. The anodically oxidized samples were prepared at the Laboratorio per la Chimica e Tecnologia dei Materiali e Componenti per l'Elettronica, Bologna.

The oxidation bath was a 5-g/liter solution of KNO_3 in ethylene-glycol with a water content less than 10%. The silicon oxide formed has then the stoichiometry SiO_2, is amorphous and has a good thickness homogeneity.[5–7]

The determination of the multiple-scattering distributions by the method outlined in Sec. II requires a precise knowledge of the composition and of the absolute amount of each component of the amorphous layer covering the crystal. For the "bare" crystals, in addition to the natural oxide, an amorphous silicon layer may arise at the oxide-crystal interface. Furthermore, a carbon layer grows at the surface of the samples during the measurements.

The absolute amount of oxygen was determined by using the $^{16}O(d,p)^{17}O^*$ nuclear reaction with 820-keV incident deuterons.[20] At this energy the contribution of nuclear reactions on the silicon substrate is negligible. The calibration was obtained using anodic Ta_2O_5 samples, their absolute oxygen content being determined by Coulometry with a ±3% precision.[24] The amount of carbon and silicon contained in the amorphous layer was then obtained by comparing in a helium backscattering aligned spectrum the surface silicon and carbon peaks to the oxygen peak and assuming the Rutherford law to hold for MeV helium. Figure 4 shows a typical channeling spectrum obtained on a bare silicon crystal with a 500 keV ^{4}He beam. Three well-resolved peaks, corresponding from right to left to silicon, oxygen, and carbon, are clearly displayed. The integrated area of these peaks can be obtained by an usual background substraction technique. The typical amount of carbon deposited was of the order of 1×10^{16} to 2×10^{16} atoms cm^{-2}. This quantity is of the same order as the total amount of silicon and oxygen atoms/cm^2 found in the disordered layer at the top of a "bare" crystal. However, as the width of the multiple scattering distributions increases with the target atomic number, it can easily be shown (for instance, by using the table

of Ref. 18) that the angular distribution of the beam entering the crystal is mainly due to the disordered silicon and oxygen (and even in most cases, as demonstrated in Sec. VI, to the beam angular divergence) and not to the deposited carbon layer.

The determination of the amount of silicon contained in the amorphous surface layer is not trivial in the case of crystals covered by thick oxide layers as in particular it is difficult to determine with precision the interface between the oxide film and the crystal. Hence we have used in this case a procedure already reported,[25] which allows one, comparing random and aligned spectra, to isolate the contribution of the silicon from the crystal and from the surface amorphous layer. Figure 5 shows a random and aligned backscattering spectrum obtained with 1.8-MeV ^{4}He on a silicon crystal covered by a 1265 Å thick SiO_2 layer. In the same figure are also represented the reconstructed spectra corresponding, respectively, to the crystal and to silicon of the SiO_2 layer. Each of these two reconstructed spectra are interesting for the data reduction: from the first one, on which the energy of the particles backscattered on the crystal surface is now well defined, it is possible, using an energy-to-depth conversion which will be discussed in Sec. V, to calculate the aligned backscattering yield as a function of depth in the crystals covered by an oxide layer; the second spectrum is of course used to determine the amount of silicon atoms in the amorphous layer.

Table I summarizes the results obtained on the composition of the amorphous surface layer for all the samples used in our experiments. The only backscattering spectra of interest for this characterization are helium spectra. No information can be extracted from the peaks areas in proton aligned spectra as the Rutherford law does not hold for backscattering of MeV protons on C, O, or Si. This can clearly be noticed in Table I where the results extracted from proton backscattering, assuming the Rutherford law, are obviously not significant. On the other hand, the silicon peak is the only peak available for spectra registered with nitrogen ions. Calling N_{ox} the number of oxygen atoms measured on a sample via the $^{16}O(d,p)^{17}O^*$ nuclear reaction and R the ratio of the number of silicon to oxygen atoms contributing to the corresponding peaks observed in an aligned helium backscattering spectrum, the absolute number of silicon atoms corresponding to the surface peak is simply $N_{Si} = RN_{ox}$. The absolute number of silicon in excess with respect to the stoichiometry SiO_2 is then

$$\Delta N_{Si} = N_{ox}(R - \tfrac{1}{2}) \quad . \tag{20}$$

The quantity ΔN_{Si} includes the contribution of ordered silicon atoms from the first layers of the crystal. Hence this contribution has to be subtracted to ΔN_{Si} in order to determine the stoichiometry of the oxide layers. A typical result of Monte Carlo calculation of this contribution is presented in Ref. 26. The number of crystal layers contributing to the surface peak is a function of the only parameter ρ/R where ρ is the rms of the thermal vibration amplitude perpendicular to the string and R the radius of the shadow cone at the second atomic layer for a Coulomb potential. One has $R = 2(Z_1 Z_2 e^2 d/E)^{1/2}$, d being the interatomic distance along the string. In our case ([110] silicon crystals) it appears that the crystal contribution to ΔN_{Si} increases from 4.4×10^{15} to 9.3×10^{15} Si atoms/cm^2 when E/Z_1 varies between 0.25 and 0.9 MeV. If these quantities are subtracted to the values ΔN_{Si} presented in Table I, it appears

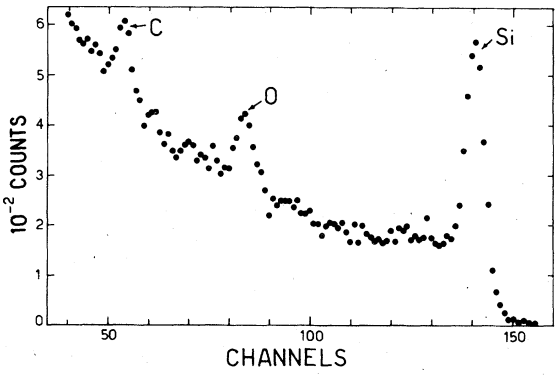

FIG. 4. [110]-aligned backscattering spectrum obtained with 0.5-MeV ^{4}He ions on a "bare" silicon crystal. $\theta_{lab} = 165°$, 1.80 keV/channel.

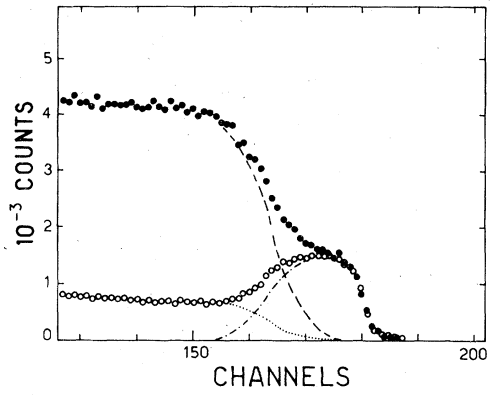

FIG. 5. Random (•) and [110]-aligned (○) backscattering spectra obtained with 1.8-MeV ^{4}He ions on a silicon crystal covered by 1265-Å SiO_2. $\theta_{lab} = 165°$, 3.62 keV/channel. The dashed and dotted lines represent, respectively, in the random and aligned cases, the contribution of the crystal to the spectra. These different contributions are calculated following the method of Ref. 25. The dash-dotted line represents the isolated contribution of the amorphous silicon.

TABLE I. Composition of the surface layers on the various samples studied. For meaning of N_{ox}, R, and ΔN_{Si}, see text.

$10^{-16}N_{ox}$ (atoms/cm^2)		0.540	5.78	14.8	37.1	57.4
R	He 500 keV	1.370	0.565	0.549	0.509	
	He 700 keV		0.575	0.543		
	He 900 keV	1.897	0.623	0.521		0.493
	He 1200 keV		0.625	0.526		
	He 1800 keV		0.685	0.535		0.490
	H 900 keV	0.932	0.594	0.427	0.326	0.320
$10^{-15}\Delta N_{Si}$ (atoms/cm^2)	He 500 keV	4.70	3.76	7.25	3.34	
	He 700 keV		4.33	6.36		
	He 900 keV	7.54	7.11	3.11		−4.02
	He 1200 keV		7.22	3.85		
	He 1800 keV		10.7	5.18		−5.74
Oxide thickness[a]	("bare" crystal)	12 Å	127 Å	326 Å	818 Å	1265 Å

[a]The thickness is calculated from N_{ox}, assuming the stoichiometry SiO_2 and a specific weight $\rho = 2.26\ g\,cm^{-3}$.

that in the limits of sensitivity of our measurements all the oxide layers can be considered as having the SiO_2 stoichiometry. For the "bare" crystal and the one covered by the thinnest oxide layer the contribution to the surface peak of the first crystal layers is dominant and the variation of ΔN_{Si} with E/Z_1 is very well observed. In this case the maximum excess of silicon with respect to SiO_2 which is found after subtraction of the crystal contribution is about 1.5×10^{15} atoms/cm^2 which is of the order of the precision of the measurements. This result is in good agreement with the results reported in Ref. 27 for similar samples and in Ref. 26 for experiments performed in ultrahigh vacuum on surface-impurity-free [100] silicon crystals.

V. AZIMUTHALLY AVERAGED YIELDS ON A BARE SILICON CRYSTAL

We report in this section the results obtained on the yields $\chi^b(\phi,x)$ which had to be inserted into Eq. (3) in order to calculate the experimental angular distributions. Figure 6 shows typical azimuthally averaged spectra registered at various tilting angles ϕ with respect to the [110] axis of a "bare" silicon crystal. These spectra are relative to 0.9-MeV incident protons.

The most immediate result that can be extracted from the data is the angular dependence of the azimuthally averaged backscattering yield near the crystal surface. The surface yields may be obtained by extrapolation of the backscattering spectra behind the surface peak. However, this procedure is not without implicit physical assumptions which will not be discussed here but may be questioned. Here we choose to consider the yield behind the surface peak. This yield is not seriously affected by dechanneling processes at least if the depth resolution is good enough (i.e., small as compared to the mean dechanneling length). This is the case for the helium spec-

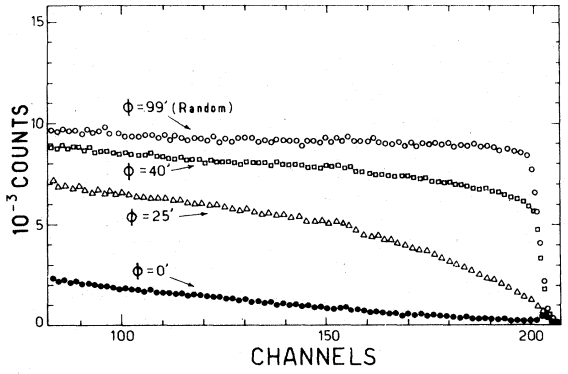

FIG. 6. Azimuthally averaged backscattering spectra registered, in the case of 0.9-MeV protons, for various tilting angles ϕ with respect to the [110] axis of a "bare" silicon crystal. $\theta_{lab} = 165°$, 2.80 keV/channel.

tra recorded in our experiments, the depth resolution always being smaller than 500 Å. We then report in Fig. 7 the backscattering yields, behind the surface peak, obtained for helium of 0.5, 0.9, and 1.8 MeV as a function of the reduced tilting angle ϕ/ψ_c where ψ_c is the critical angle for channeling proposed by Lindhard[28]:

$$\psi_c = \left(\frac{2Z_1Z_2e^2}{Ed}\right)^{1/2}, \tag{21}$$

d being here the interatomic spacing along the [110] direction.

The three experimental angular dips of Fig. 7 are superimposed. The striking feature, which was also noted in Ref. 10 is that no shoulder effect appears when azimuthally averaged yields are measured. The shoulders usually observed at fixed azimuthal positions are hence clearly due to planar channeling effects. From the theoretical point of view shoulder effects are predicted in axial dips, following a calculation performed in the half-way plane approximation, for crystals at low temperature.[29] At higher temperature the shoulder effect damps out and the half-way plane approximation leads to results identical to the continuum string approximation.[28] We hence compare in Fig. 7 the experimental dips to the angular dip calculated using the continuum string approximation and

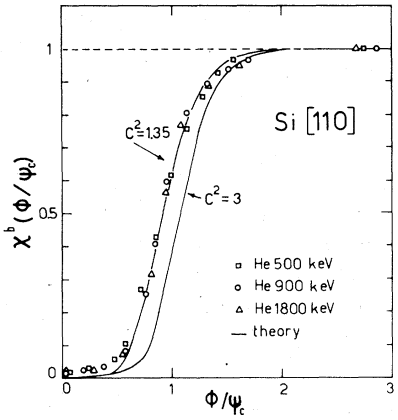

FIG. 7. Normalized backscattering yields behind the surface peak as a function of the reduced tilting angle ϕ/ψ_c for ^{4}He beams of various energies. The continuous lines are the angular scans calculated from Eq. (22) for two different values of the parameter C^2.

assuming statistical equilibrium. It can be easily shown that, if one uses in the calculations the standard interatomic potential proposed by Lindhard,[17] the yield $\chi^b(\phi,0)$ obtained with this hypothesis is given by

$$\chi^b(\phi,0) = \int_0^{r_0} \frac{2r\,dr}{r_0^2 - C^2a^2/[(1+C^2a^2/r^2)\exp(2\phi^2/\psi_c^2)-1]} \times \frac{\exp\{-(C^2a^2/2\rho^2)/[(1+c^2a^2/r^2)\exp(2\phi^2/\psi_c^2)-1]\} - \exp(-r_0^2/2\rho^2)}{1-\exp(-r_0^2/2\rho^2)} . \tag{22}$$

ρ is the rms value of thermal vibrations in the Debye Waller model; r_0 is the radius of the unit cell around an atom. The parameter C^2 is an adjustable constant introduced in the standard interatomic potential and usually taken equal to 3. With this value of C^2, there is a significant discrepancy (about 20%) between the width of the experimental and calculated dips. The best agreement is obtained when the value $C^2=1.35$ is introduced in Eq. (22). This value has obviously no physical meaning and in particular does not give any information about the interatomic potential: C^2 was here used as a fitting parameter. The disagreement between the experimental results and the calculations with $C^2=3$ questions at least as much the continuum model approximation and the statistical equilibrium hypothesis than the interatomic potential. Moreover, it must be pointed out that the value of the yield $\chi^b(\phi,0)$ for $\phi=0$ extracted from Eq. (22) is independent of C^2

$$\chi^b(0,0) = \int_0^{r_0} \frac{2r\,dr}{r_0^2-r^2} \frac{\exp(-r^2/2\rho^2)-\exp(-r_0^2/2\rho^2)}{1-\exp(-r_0^2/2\rho^2)} \simeq 2\rho^2/r_0^2 = 2Nd\pi\rho^2 . \tag{23}$$

This value is significantly lower than the experimental one (0.7% versus about 2%).

Depth dependence

To analyze the change of the angular dip with the penetration depth, it is necessary to establish an energy-to-depth conversion scale. At the energies used in the present experiment, the ratio between channeling and random stopping powers is near to unity. However, even if the value of this ratio is taken as equal to 0.5 (which may be the limit case for 900-keV protons), it can be shown that the correction

on the depth scale due to the fact that the particles are channeled in part of their way into the crystal does not exceed 10%. For this reason we decided to neglect this correction and to use the random stopping power for the energy to depth conversion. This choice having also been done by other authors, a direct comparison of our results with theirs is possible. We used the stopping-power values for protons, helium, and nitrogen ions tabulated in Ref. 30. Figure 8 represents angular dips corresponding to various penetration depths in the case of 900-keV protons. From this figure the depth dependence of the minimum yield $\chi^b(0,x)$ and of the width of the angular scans can be extracted. Figure 9 shows the dependence of χ^b at $\phi=0$ (minimum yield) on the reduced penetration depth $\bar{x}=Z_1x/\bar{E}$ for various ions and energies. $\bar{E}=E(x/2)$ is the mean energy, in their way into the crystal, of the particles backscattered at depth x. A difference appears in Fig. 9 between protons and He-N data; in the case of these last ions, a linear dependence on the reduced depth seems to be valid, whereas the stronger dependence displayed by protons seems better fitted by an exponential law. It must be pointed out that the reduced depth $\bar{x}$ has a physical meaning only if the nuclear multiple scattering dominates the dechanneling processes. The discrepancy observed in this scale between protons and other particles would then illustrate the importance of the particle-electron interaction in dechanneling. We also report in Fig. 9 the results and calculations performed by Pedersen *et al.*[31] in the case of 1.6-MeV proton dechanneling in [110] silicon. These results are in remarkable agreement with our data on 0.9-MeV protons.

As shown in Fig. 8 the dechanneling processes also strongly affect the width of the angular scans. This

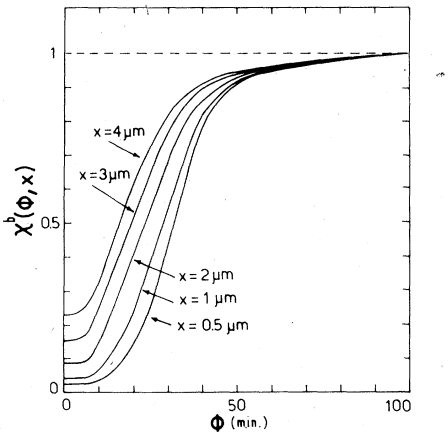

FIG. 8. Experimental [110] silicon angular scans for 0.9-MeV protons backscattered at various depths below the surface.

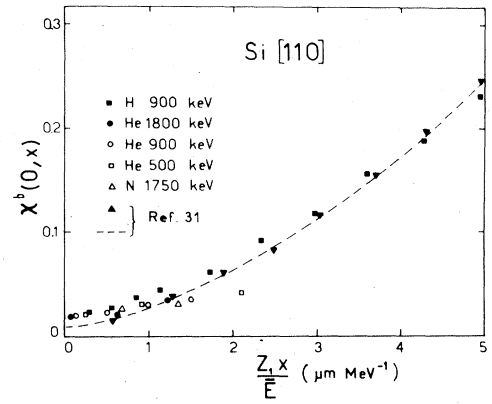

FIG. 9. Minimum backscattering yields, registered for different ions at various energies, as a function of the reduced penetration depth. The results and calculations of Pedersen *et al.*[31] in the case of 1.6-MeV protons are also reported.

effect may be characterized by the depth dependence of the HWHM $\psi_{1/2}$ of the scans. In Fig. 10 we have plotted the values of the ratio $\psi_{1/2}(x)/\psi_c(x)$ as a function of the reduced depth $\bar{x}$. $\psi_c(x)$ has been calculated from Eq. (21) by taking into account the energy loss of the incident particle at depth x. Our results, presented in Fig. 10, exhibit the same behavior for all the particles and energies studied. We have also reported in this figure the results obtained by Davies *et al.*[32] for 3-MeV protons in [110] silicon. At high reduced depths these results are in good agreement with ours, however the reduced half angle measured in Ref. 32 near the crystal surface is significantly lower than all the experimental points of the present work.

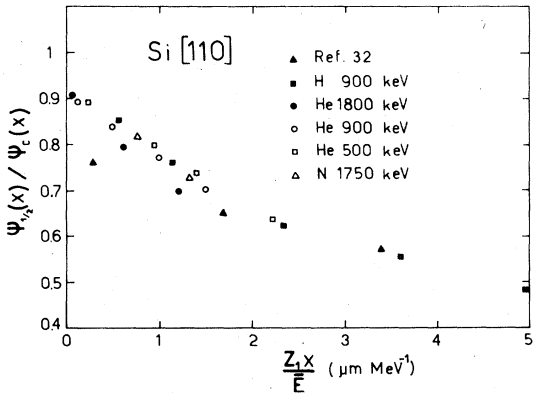

FIG. 10. Dependence on the reduced penetration depth of the HWHM $\psi_{1/2}(x)$ of the experimental angular scans, normalized to the Lindhard critical angle $\psi_c(x)$, for various particles and energies. We also report the results obtained in Ref. 32 for 3-MeV protons.

The experimental results presented in this section about channeling of MeV light ions in silicon were essential for the interpretation of our multiple-scattering measurements. They have also their proper interest as precise and detailed experimental data are useful, in particular for the understanding of dechanneling processes.

VI. DETERMINATION OF THE EXPERIMENTAL ANGULAR DISTRIBUTIONS

A. Procedure used

The general outline of the method was given in Sec. II. Here we discuss the details of the procedure used to obtain the angular distributions $2\pi\phi F(\phi)$ from Eq. (3), the quantities $\chi^{ox}(x)$ and $\chi^{b}(\phi,x)$ being known from the experimental results. We will also set the precision and limits of the method.

It must first be pointed out that even though Eq. (3) contains factors depending on the penetration depth in the crystal, the energy-to-depth conversion plays *no* role in limiting the precision of the method. This is of crucial importance as this conversion has not a strict physical meaning in channeling experiments. In fact, Eq. (3) could have been written by replacing the depth dependence of χ by its dependence on the detected energy as directly measured in a backscattering spectrum. Our choice of a depth scale just appeared more convenient for plotting the whole set of results. Moreover this choice is interesting as it leads to results on the influence of amorphous layers on the dechanneling as a function of penetration depth into a crystal [study of the parameter $\chi^{ox}(x)$].

It is possible to obtain an analytical solution of Eq. (3) by assuming that the angular scans can be approximated at all depths in the "bare" crystal by square wells characterized by two parameters only: $\chi^{b}_{\min}(x)$ and $\psi_{1/2}(x)$. This improvement and extension of the treatment of Ref. 10 was already used in Ref. 13. The yields $\chi^{b}(\phi,x)$ are given by

$$\chi^{b}(\phi,x)=\begin{cases}\chi^{b}_{\min}(x) \text{ for } \phi \leq \psi_{1/2}(x)\\ 1 \text{ for } \phi > \psi_{1/2}(x)\end{cases} . \tag{24}$$

Introducing the weight of the angular distribution between two angles ϕ_i and ϕ_j as

$$P(\phi_i,\phi_j)=\int_{\phi_i}^{\phi_j} 2\pi\phi F(\phi)\,d\phi , \tag{25}$$

one has

$$P(\psi_{1/2}(x_i),\psi_{1/2}(x_j))=\frac{\chi^{ox}(x_j)-1}{\chi^{b}_{\min}(x_j)-1}-\frac{\chi^{ox}(x_i)-1}{\chi^{b}_{\min}(x_i)-1} . \tag{26}$$

Hence we can construct a histogram associated with the angular distribution $2\pi\phi F(\phi)$ which fits the experimental results. This is done in Fig. 11 in the case of 0.9-MeV protons having passed through 1265 Å of SiO_2. In the same figure we report the histogram constructed with the data of Ref. 18 by assimilating the SiO_2 layer to a monoatomic target with $\bar{Z}_2=10$ containing the same number of scattering centers. The screening radius used in the conversion between real and reduced coordinates is the one proposed by Lindhard[17]:

$$a=0.8853a_0(Z_1^{2/3}+Z_2^{2/3})^{-1/2} , \tag{27}$$

a_0 being the Bohr radius of the hydrogen atom.

The tabulated angular distribution chosen was calculated using a scattering cross section corresponding to the Thomas-Fermi potential: this choice is not critical as for the thicknesses of interest in this paper the angular distribution calculated using either Thomas-Fermi or Lenz-Jensen potentials are nearly identical. The experimental histogram corresponds to an angular distribution somewhat wider than predicted; however the discrepancy does not exceed 15% and may be attributed to the square-well approximation used in the data reduction. We decided hence not to use this approximation and to take into account the real shape of the angular scans. In this situation it is far more convenient to use a fitting procedure, i.e., to check whether a given function $F(\phi)$ satisfies Eq. (3) for all values of x. The fitting procedure is particularly justified in our case as we had at our disposal tabu-

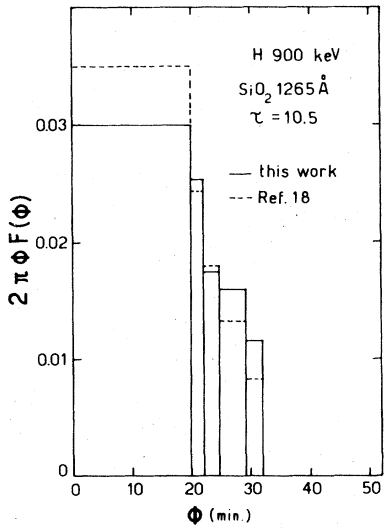

FIG. 11. Comparison of the histogram of an angular distribution obtained from our experimental results, using the square-well approximation, to the histogram calculated from Ref. 18 for an equivalent monoatomic target with $\bar{Z}_2=10$.

lated starting trial functions which, as demonstrated in Fig. 11, were rather close to the best-fitting function.

The fits were obtained using the MATEK 1026 computer on line with the accelerator. The trial angular distributions and the angular scans $\chi^b(\phi,x)$ were characterized by numerical values for various angles ϕ_i. The width of an angular step $[\phi_i, \phi_{i+1}]$ was always small enough to ensure the validity of linear approximation of the functions $2\pi\phi F(\phi)$ and $\chi^b(\phi,x)$ in the interval. For a given trial function $F(\phi)$, the yield $\chi^{ox}(x)$ is then, from Eq. (3)

$$\chi^{ox}(x) = 2\pi \sum_i (\phi_{i+1} - \phi_i) \{\tfrac{1}{6}[\phi_i F(\phi_i)\chi^b(\phi_{i+1},x) + \phi_{i+1}F(\phi_{i+1})\chi^b(\phi_i,x)] + \tfrac{1}{3}[\phi_i F(\phi_i)\chi^b(\phi_i,x) + \phi_{i+1}F(\phi_{i+1})\chi^b(\phi_{i+1},x)]\} \quad . \tag{28}$$

B. Limits of the method

As we search for the angular distributions by checking their influence on the backscattering yields in a single crystal, valuable information can obviously only be obtained if the angular dependence of these backscattering yields extends over an angular domain (which can be characterized by $\psi_{1/2}$) of the same order of magnitude as the width of the body of the angular distributions. In this case the shape of the body of the distributions can be analyzed. On the contrary, the part of the distributions which extends towards angles greater than the width of the angular scans cannot be analyzed in shape; the only quantity which can be obtained for this part is its relative weight.

If one wants to study the multiple scattering of a given particle of given energy through a given material, the range of the material thickness is restricted by the condition set above. The only way to change the thickness domain that can be studied is to choose a well adapted value of $\psi_{1/2}$. This can in principle be done in two ways. $\psi_{1/2}$ is proportional to (Z_c/d), where Z_c is the atomic number of the crystal atoms. Hence one can adjust $\psi_{1/2}$ by using the best adapted crystallographic direction, i.e., by adjusting d. Another possibility, not always technically available, would be to form or deposit the material to be studied on a well chosen single crystal looking hence for the best adapted Z_c. If one is more interested in a study of $2\pi\phi F(\phi)$ as a function of the thickness than as a function of the nature of the scattering material, a proper choice of this material would on the contrary adapt the width of the body of the searched distribution to $\psi_{1/2}$. The remaining parameters available are the nature and energy of the scattered particles as the scaling factor for the angular distributions and $\psi_{1/2}$ are, respectively, Z_1/E and $(Z_1/E)^{1/2}$.

In our practical case we were restricted to MeV light ions and no valuable information could be expected for SiO_2 thicknesses smaller than a few hundred angstroms. As discussed in Sec. II, a major improvement of the method is obtained when taking into account the dechanneling processes. This can only be achieved if there is a significant change of the angular scans $\chi^b(\phi,x)$ in the domain of penetration depths x in the crystal that can be studied. In regard to this point, the case of MeV protons is particularly favorable as, owing to their low stopping power, a large penetration depth domain can be explored. This is illustrated in Fig. 12 where the angular scans $\chi^b(\phi,x)$ obtained for 900-keV protons are plotted along with the theoretical angular distributions calculated for various thicknesses of SiO_2. It can clearly be observed on this figure that, if it appears hopeless to analyze the angular distribution corresponding to 127 Å of SiO_2, rather precise information can be

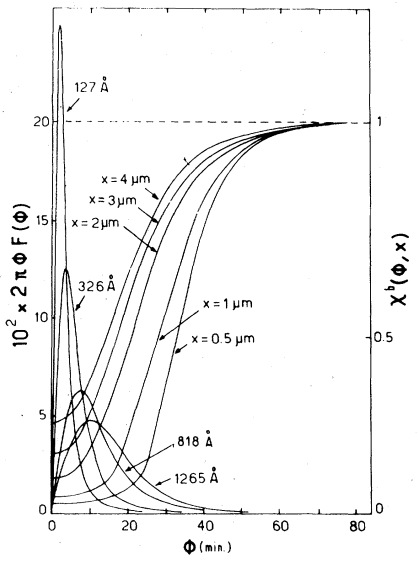

FIG. 12. Angular distributions for various SiO_2 thicknesses (left scale) and 0.9-MeV proton angular scans at various penetration depths into the crystal (right scale) are compared in width in order to observe the precision and limits of the method.

expected for distributions corresponding to SiO_2 thicknesses between 500 and 1500 Å.

There are two other limitations in our experiments. The first one is related to the beam angular divergence which was measured to be 0.5 mrad HWHM. The second limitation is set by the existence of unwanted layers on the "bare" and oxidized samples. These layers are, as discussed in Sec. IV, of two types: (i) carbon deposited during the analysis; (ii) natural oxide on the bare samples. It can be shown that in all our experiments the contribution of the beam angular divergence dominates. This is due to the fact that for the light ions and relatively high energies used, the scattering cross sections are small, leading hence to very narrow angular distributions after crossing the unwanted layers which thicknesses are reported in Sec. IV. The angular distribution of the incident beam is different in shape from the multiple-scattering distributions. However, in regard to order of magnitude and in order to estimate the experimental uncertainties it is interesting to evaluate the thicknesses of the SiO_2 layers which would lead to angular distributions comparable in width (HWHM) to the overall unwanted beam spread. We found that this thickness varies from about 130 Å in the case of 900-keV protons to about 40 Å for 500-keV helium and 1750-keV nitrogen ions. In the case of the oxidized samples, a first-order correction may be simply obtained by adding the SiO_2 thicknesses defined above to the SiO_2 thicknesses measured by nuclear microanalysis; this treatment is satisfactory if the corrective term which can be estimated with a 20% uncertainty, is small as compared to the overall thickness. This implies that trustful quantitative results can only be obtained here for SiO_2 layers thicker than 500 Å. It is interesting to note that this lower thickness limit is the same as the one obtained in the preceding discussion where the relative widths of the angular scans and multiple-scattering distributions were compared.

It is more difficult to take into account the effect of the beam angular divergence and of the unwanted layers on the assumed "bare" crystal. The experimental yields $\chi^b(\phi,x)$ measured are somewhat different from the yields corresponding to a really bare crystal, and to a parallel incident beam, which should be inserted in Eq. (3). However, an estimation of the contribution of this effect on the measured $\chi^b_{\text{exp}}(\phi,x)$ may be attempted using the square-well approximation described in Sec. VI A.

As the weight in the $[0, \psi_{1/2}(x)]$ domain of the angular distribution corresponding to the overall unwanted beam spread is known, one can calculate, using this approximation, a "theoretical" value $\chi^b(0,x)$ from the experimental value $\chi^b_{\text{exp}}(0,x)$. The result is

$$\chi^b(0,x) = 1 - [1 - \chi^b_{\text{exp}}(0,x)]/P(0, \psi_{1/2}(x)) \quad . \tag{29}$$

It is reasonable to assume that the half-width $\psi_{1/2}(x)$ of the angular scans is less affected by the unwanted beam spread than the values $\chi^b(0,x)$. We hence have inserted the experimental values $\psi_{1/2}(x)$ in Eq. (29). The values $\chi^b(0,x)$ obtained in this way were used to reconstruct corrected angular scans, which were introduced in data reduction.

The different corrections described in this section do not lead, all together, to more than 5% to 10% effects on the widths of the angular distributions obtained from the experimental results in the case of SiO_2 layers of thicknesses larger than about 500 Å. As indicated above, uncertainties on the corrections are of the order of 20%; consequently the precision on the widths of the angular distributions found in this work is of the order of 2%.

VII. COMPARISON OF THE EXPERIMENTAL AND PREDICTED ANGULAR DISTRIBUTIONS

Typical fits of the yields $\chi^{ox}(x)$ are presented in Fig. 13. These fits were obtained as discussed in Sec. VI by inserting appropriate functions $F(\phi)$ in Eq. (3). The theoretical functions $F(\phi)$ are related to the functions $f_1(\tau, \tilde{\phi})$ tabulated in Ref. 18 by

$$2\pi\phi F(\phi)\,d\phi = \tilde{\phi} f_1(\tau, \tilde{\phi})\,d\tilde{\phi} \tag{30}$$

In all cases it appeared possible to fit the yield curves $\chi^{ox}(x)$ over the whole range of experimentally available penetration depths x with functions $F(\phi)$ calculated by inserting in Eq. (30) a function f_1 obtained by a simple contraction or dilatation by an appropriate factor β of a starting function tabulated in Ref. 18. This corresponds simply to a change in scale and hence the shape of the tabulated distributions is satisfactory in regard to our experimental results. Our discussion will hence be restricted to the width of the distributions leading to the best fit.

As discussed in Sec. III, for a given reduced thickness τ one may consider that the dominant collisions in regard to their influence on the body of the multiple-scattering distribution arise from a restricted domain of impact parameters to which can be associated a given power potential $R^{-1/m}$. For small variations of τ the shape of the angular distribution is hence conserved and the scaling factor for the width of the body of the distribution is $\tau^{1/2m}$. Hence if the reduced thickness corresponding to the starting tabulated distribution is τ, the distribution leading to the best fit and obtained by dilatation or contraction corresponds, if β is closed enough to unity (this was always the case in our data reduction) to a distribution expected for a thickness $\tau\beta^{2m}$. The values of m which are appropriate for the thicknesses studied here are, as shown in Sec. III, of the order of 0.7.

The quality of the fits presented in Fig. 13 is significantly affected by a modification of 1% of the

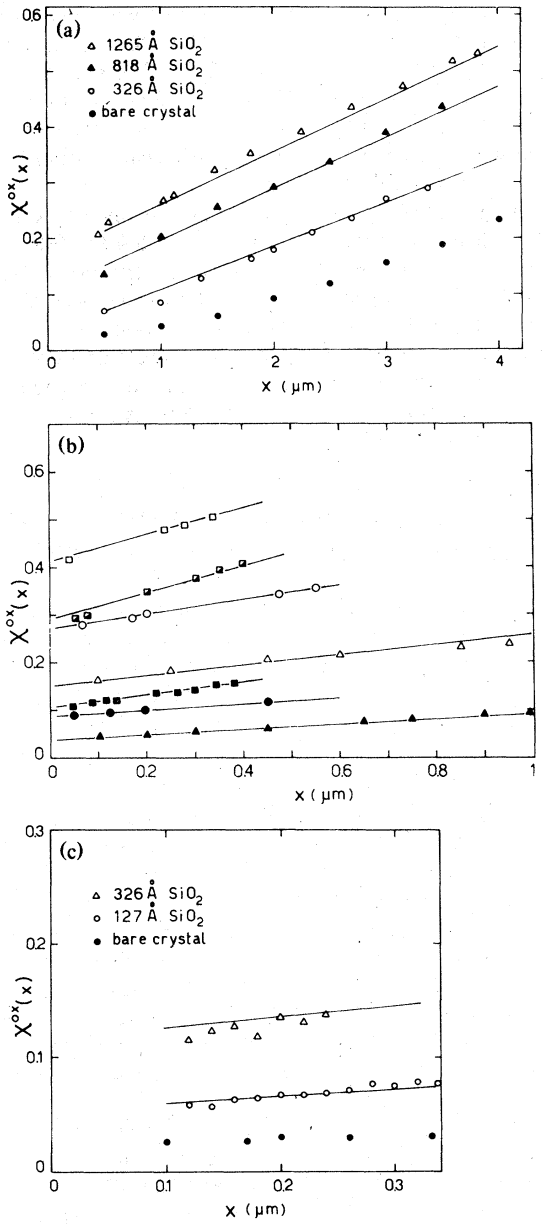

FIG. 13. Fit of the depth dependence of the minimum yields for oxidized crystals leading to the determination of the angular distributions. The points are the experimental yields whereas the continuous lines are the calculated fits. (a) Case of 0.9 MeV protons. (b) Case of ^{4}He ions. Squares, circles, and triangles refer, respectively, to 0.5-, 0.9-, and 1.8-MeV incident energies; open and full symbols refer, respectively, to 1265-Å and 326-Å SiO_2 layers. The symbol ◪ refers to 818-Å SiO_2 layer. (c) Case of 1.75-MeV nitrogen ions.

parameter β. The widths of the angular distributions fitting our results are hence determined with this precision; the corresponding precision on the associated reduced thicknesses which varies like β^{2m} is then 1.5%.

An appropriate parameter to characterize the width of the angular distribution is the FWHM $\tilde{\phi}_{1/2}$ of the function $f_1(\tau, \tilde{\phi})$. We report in Fig. 14 a graph of the theoretical dependence $\tilde{\phi}_{1/2}(\tau)$ and, plotted along, the set of points corresponding to our experimental results. The ordinate of these points correspond to the value $\tilde{\phi}_{1/2}$ leading to the best fit and their abscissas to the values of τ obtained from our experimental determination of the target thicknesses, taking also into account, in the way described in Sec. VI, the overall unwanted beam spread.

The screening radius a intervenes in the relations between the real and reduced angles and thicknesses [see Eqs. (7) and (8)]. As usually done in literature, the Lindhard screening radius was used in order to plot the experimental points in Fig. 14. This screening radius was calculated for a monoatomic target with $\bar{Z}_2 = 10$, which was shown to be equivalent to SiO_2. We also report in Fig. 14 results from Högberg *et al.*[33] relative to hydrogen and helium ions of about 40 keV in carbon foils. A reasonable agreement between theory and all the experimental results is observed. However, a striking feature is that for $\tau \gtrsim 5$, i.e., in all the cases for which our measurements were sufficiently accurate, the experimental values $\tilde{\phi}_{1/2}$ are systematically about 10% higher than predicted. This is in agreement with the results of Ref. 33 and more generally with various different measurements performed for hydrogen and helium ions.[34,35] An explanation of this effect may be attempted in our particular case. Our experiments were performed with hydrogen and helium ions at energies greater than 500 keV. At these energies the mean charge associated to the charge-state equilibrium of these particles

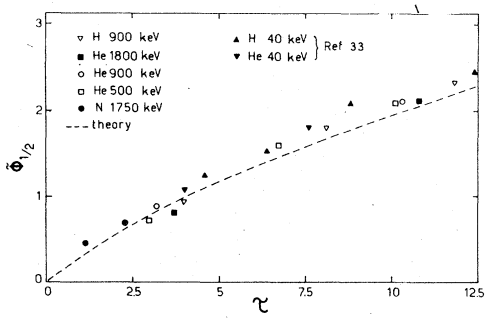

FIG. 14. Comparison between the reduced widths of experimental and theoretical angular distributions for various reduced thicknesses τ. The experimental results are obtained with various particles and energies. The reduced thicknesses and widths are calculated using the Lindhard screening radius for $\bar{Z}_2 = 10$. Results from Ref. 33 are also reported.

in matter is near its maximum value which corresponds to completely stripped particles. It appears hence more convenient to use the atomic screening radius corresponding to the target atom:

$$a' = 0.8853 a_0 Z_2^{-1/3} \quad . \tag{31}$$

If one changes the value of the screening radius from a to a' for a given thickness of matter Nx, the reduced thickness will become [see Eq. (7)]:

$$\tau' = \tau (a'/a)^2 \tag{32}$$

The scaling factor in width is $\tau^{1/2m}$ with a value m well adapted for thicknesses of the order of τ. Hence the change in reduced angle width will be

$$\tilde{\phi}^{a'}_{1/2} = \tilde{\phi}^{a}_{1/2} (a'/a)^{1/m} \quad , \tag{33}$$

and the change in width in the laboratory system will be [see Eq. (8)]

$$\phi^{a'}_{1/2} = \phi^{a}_{1/2} (a'/a)^{1/m-1} \quad . \tag{34}$$

Equation (34) shows that if m is significantly lower than 1, the choice of a screening radius seriously affects the comparison between experimental results and the theory. In our case, the ratio $\phi^{a'}/\phi^{a}$ varies as $(a'/a)^{0.4}$. The atomic screening radius $a_{TF} = a' = 0.217$ Å for $\bar{Z}_2 = 10$ is, respectively, 15% to 10% greater than the Lindhard screening radius corresponding to helium and proton ($a_L^{He} = 0.188$ Å and $a_L^{H} = 0.197$ Å). The theoretical angular widths (for a given thickness Nx) expressed in real angles are hence broadened from 5% to 7% when the atomic screening radius is used; this significantly improves the agreement between experimental results and theory. This appears clearly in Fig. 15 where the theoretical graph $\tilde{\phi}^{a'}_{1/2}(\tau)$ is compared to our experimental results, expressed in reduced coordinates by using the screening radius a' of Eq. (31). In this figure, we report only the results corresponding to $\tau > 5$ which were shown to be determined with precision. The discrepancy between the ordinates of the experimental points and the theoretical curve never exceeds 3%. This is very satisfactory in regard to the various uncertainties reported in this paper and which affect the position of the experimental points.

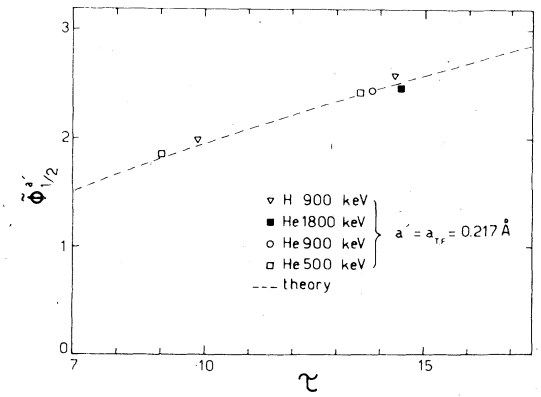

FIG. 15. Comparison between the reduced widths of experimental and theoretical angular distributions for various reduced thicknesses τ. The experimental results for protons and ^{4}He are reported in reduced coordinates using for the conversion the Thomas-Fermi screening radius of the mean target atoms ($\bar{Z}_2 = 10$).

The agreement illustrated in Fig. 15 is not a definite indication that the atomic screening radius of the target atom is the most appropriate to describe the collision with a completely stripped ion. In fact, the electronic surrounding of a target atom during a collision is modified by the presence of the particle. It would then be reasonable to guess that a well adapted screening radius should have a value in between the value proposed by Lindhard, which is assumed to describe an atom-atom collision, and the value corresponding to the screening of the target atom alone. The definite improvement obtained in our case by taking into account the fact that the incident ions are stripped in matter is, however, certainly significant. Such an improvement cannot be reached for the results of Refs. 33–35 where low-energy (around 50 keV) proton and helium ions, which cannot be considered as stripped, were used. In Ref. 34, however, considering that the Thomas-Fermi potential is perhaps not perfectly appropriate in the case of ions of low atomic number, the authors have adjusted their results to the theory by using an *ad hoc* value of the screening radius which was hence considered as a fitting parameter.

The agreement between the results of the present work and the theory indicates that the basic hypotheses of this theory are appropiate for multiple scattering in the targets used in our experiments. In particular, the hypothesis that multiple scattering may be described by a series of independent binary collisions obeying Poisson statistics appears to be a good approximation for amorphous solids in the range of thicknesses studied here.

ACKNOWLEDGMENTS

This work was supported by the Centre National de la Recherche Scientifique (Recherche Cooperative sur Programme No. 157) and the Consiglio Nazionale delle Ricerche. The authors greatly appreciated the efficient help of E. Girard and J. Moulin for electronic and electromechanical problems, especially in connection with the digitally controlled goniometer. We are indebted to M. Vidal for designing the beam chopper which appeared as an indispensable tool for

these experiments and many others. The assistance of E. d'Artemare for problems related to the accelerator was most useful. We wish to thank P. Mazzoldi for his constant interest during the work. The enlightening discussions with G. Amsel, in particular about the basis of the multiple-scattering theory, were of great help for our comprehension of the problem.

[1]N. Bohr, K. Dan. Vidensk. Selsk. Mat. Fys. Medd. 18, 8 (1948).
[2]H. H. Andersen, J. Bøttiger, H. Knudsen, P. Møller Petersen, and T. Wohlenberg, Phys. Rev. A 10, 1568 (1974).
[3]H. Knudsen and H. H. Andersen, Nucl. Instrum. Methods 136, 199 (1976).
[4]E. Rimini, E. Lugujjo, and J. W. Mayer, Phys. Lett. A 37, 157 (1971).
[5]A. G. Revesz, Phys. Status Solidi 24, 115 (1967).
[6]M. Croset, E. Petreanu, D. Samuel, G. Amsel, and J. P. Nadai, J. Electrochem. Soc. 118, 717 (1971).
[7]G. Restelli, F. Girardi, F. Mousty, and A. Ostidich, Nucl. Instrum. Methods 112, 581 (1973).
[8]G. Amsel and D. Samuel, Anal. Chem. 39, 1689 (1967).
[9]D. Schmaus, thesis, (Paris, 1977) (unpublished).
[10]E. Lugujjo, and J. W. Mayer, Phys. Rev. B 7, 1782 (1973).
[11]L. Meyer, Phys. Status Solidi 44, 253 (1971).
[12]E. Rimini, E. Lugujjo, and J. W. Mayer, Phys. Rev. B 6, 718 (1972).
[13]S. U. Campisano, G. Foti, F. Grasso, and E. Rimini, Phys. Rev. B. 8, 1811 (1973).
[14]W. Bothe, Z. Phys. 5, 63 (1921).
[15]P. Sigmund, K. Dan. Vidensk. Selsk. Mat. Fys. Medd. 39, 11 (1977).
[16]P. Sigmund, in Proceedings of the Seventh International Conference on Atomic Collisions in Solids, Moscow, 1977 (unpublished).
[17]J. Lindhard, V. Nielsen, and M. Scharff, K. Dan Vidensk. Selsk. Mat. Fys. Medd. 36, 10 (1968).
[18]P. Sigmund and K. B. Winterbon, Nucl. Instrum. Methods 119, 541 (1974).
[19]A. D. Marwick and P. Sigmund, Nucl. Instrum. Methods 126, 317 (1975).
[20]G. Amsel, J. P. Nadai, E. d'Artemare, D. David, E. Girard, and J. Moulin, Nucl. Instrum. Methods 92, 481 (1971).
[21]A. L'Hoir, C. Cohen, and G. Amsel, in *Ion Beam Surface Layer Analysis*, edited by O. Meyer, G. Linker and F. Käppeler (Plenum, New York, 1976), p. 965.
[22]F. Abel, G. Amsel, M. Bruneaux, C. Cohen, and A. L'Hoir, Phys. Rev. B 13, 993 (1976).
[23]M. Vidal, thesis, (Conservatoire National des Arts et Metieurs, Paris, 1972) (unpublished).
[24]G. Amsel, J. P. Nadai, C. Ortega, S. Rigo, and J. Siejka, Nucl. Instrum. Methods 149, 705 (1978).
[25]A. Armigliato, G. G. Bentini, G. Ruffini, G. Battaglin, G. Della Mea, and A. V. Drigo, Nucl. Instrum. Methods (to be published).
[26]R. L. Kauffman, L. C. Feldman, P. J. Silverman, and R. A. Zuhr, Appl. Phys. Lett. 32, 93 (1978).
[27]G. Della Mea, A. V. Drigo, S. Lo Russo, P. Mazzoldi, S. Yamaguchi, and G. G. Bentini, Appl. Phys. Lett. 26, 147 (1975).
[28]J. Lindhard, K. Dan. Vidensk. Selsk. Mat. Fys. Medd. 34, 14 (1965).
[29]J. U. Andersen, K. Dan. Vidensk. Selsk. Mat. Fys. Medd. 36, 7 (1967).
[30]L. C. Northcliffe and R. F. Schilling, Nucl. Data Tables 7, 233 (1970).
[31]M. J. Pedersen, J. U. Andersen, D. J. Elliott, and E. Laegsgaard, *Atomic Collisions in Solids*, edited by S. Datz, B. R. Appleton, and C. D. Moak, (Plenum, New York, 1975), p. 863.
[32]J. A. Davies, J. Denhartog, and J. L. Whitton, Phys. Rev. 165, 345 (1968).
[33]G. Högberg, H. Norden, and H. G. Berry, Nucl. Instrum. Methods 90, 283 (1970).
[34]F. Bernhard, P. Krygel, R. Manns, and S. Schwabbe, Radiat. Eff. 13, 249 (1972).
[35]H. C. Schäffler, Max-Planck-Institut für Plasmaphysik, Garching, Report No. IPP 9/14 (1973) (unpublished).